

Contents lists available at ScienceDirect

# Journal of the Mechanics and Physics of Solids

journal homepage: www.elsevier.com/locate/jmps





# Solving transient problems in soft Elasto-Hydrodynamic lubrication

Haibin Wu<sup>a</sup>, Chung-Yuen Hui<sup>a,c,\*</sup>, Anand Jagota<sup>b</sup>

- a Department of Mechanical and Aerospace Engineering, Field of Theoretical and Applied Mechanics, Cornell University, Ithaca, NY 14853, USA
- b Departments of Bioengineering and of Chemical & Biomolecular Engineering, 111 Research Drive, Lehigh University, Bethlehem, PA 18015, USA
- <sup>c</sup> Global Station for Soft Matter, GI-CoRE, Hokkaido University, Sapporo, Japan

# ARTICLE INFO

# Keywords: Transient elasto-hydrodynamics Lubrication Numerical Method Soft matter

#### ABSTRACT

Many important problems in elasto-hydrodynamic lubrication arise when one of the contacting bodies is elastically soft. An example is the squeezing of a thin liquid film between a rigid sphere/cylinder and a soft elastic substrate, in which the sphere may not be sliding and be subjected only to normal loads (stationary contact), or it can be sheared at the same time and undergo steady or non-steady sliding. These problems are notoriously difficult to solve for soft solids under large loads and thin lubricant films. For this reason, indentation and sliding problems have usually been analyzed separately, and solutions for transient sliding problems are few. Here we develop a numerical method that avoids difficult-to-converge iterative methods and is able to solve both normal indentation and/or transient sliding lubrication problems. The scheme is fully automatic, stable, and efficient and requires only a linear matrix equation to be solved at every time step. We present solutions of two transient sliding problems: in the first of which, a rigid sphere undergoes transient normal lubricated contact followed by transient sliding on an elastic half space. In the second, a rigid cylinder undergoes transient lubricated sliding on an elastic foundation.

# 1. Introduction

Lubricants, for example a thin layer of oil on contacting surfaces, reduce friction and adhesion, and prolong the life of engineering components such as gears and pistons. An important class of problems in lubrication is when a coherent liquid film exists between two contacting surfaces and the hydrodynamic pressure is sufficiently large to support the normal and shear load without solid-solid contact. Elasto-hydrodynamic lubrication (EHL) is an important subclass of this problem in which the pressure is sufficient to cause significant *elastic* deformation in the solids. EHL theory has been applied extensively, traditionally, with a heavy emphasis on stiff metal contacts such as in bearings (Okrent, 1961; Tzeng and Saibel, 1967) and pistons (Martz, 1947; Mcgeehan, 1978). EHL theory is also of great importance to the understanding of filtration, coagulation and adhesion of small particles (Davis, 1984; D'Ottavio and Goren, 1982; Esmen et al., 1978). Of particular recent interest is the lubricated contact between soft elastic materials and a hard surface, such as the sliding of rubbery tires or shoe soles on wet roads (Hutt and Persson, 2016; Li et al., 2006), and the lift forces of cylinders near compliant walls (Bertin et al., 2021; Essink et al., 2021; Saintyves et al., 2016). Soft structured surfaces have been designed to increase friction during lubricated sliding (Mourier et al., 2006; Moyle et al., 2022, 2020, 2018; Rivetti et al., 2017; Touche et al., 2016; Wu et al., 2022b, 2019). Lubrication between a soft and hard surface (soft lubrication) is also important to the

E-mail address: ch45@cornell.edu (C.-Y. Hui).

<sup>\*</sup> Corresponding author.

proper functioning of joints, eyelids and eyeballs with contact lenses (Dowson and Jin, 1986; Jin and Dowson, 2005).

Conventional problems in EHL can be roughly grouped into two classes: In the first, the thin liquid film is squeezed by two approaching cylinders (line contact) or spheres (point contact). Previous work in this part includes: (Christensen, 1962), (Herrebrugh, 1970), (Lee and Cheng, 1973) (Hamrock and Dowson, 1976a), (Evans, 1981), (Davis et al., 1986) and (Wang et al., 2017). These problems are intrinsically transient, i.e., time-dependent. The second class considers steady state rolling or sliding of spheres or cylinders. Here, the steady state assumption allows one to bypass the difficulty of solving a transient problem. The governing equation for EHL is the nonlinear Reynolds equation. This equation is often coupled to the elasticity of the contacting bodies via an integral equation which relates the elastic displacements to the hydrodynamic pressure. Because soft elastohydrodynamics problems are difficult to solve, little attention has been paid to general transient problems. There is therefore a need for a method that can solve a broad range of EHL problems.

To the best of our knowledge, the computational techniques designed to solve these coupled problem all require some iteration. In the traditional iteration approach, one starts with the pressure field, and the shape of the liquid film is calculated in two different ways: one by elasticity and the second by inverting the Reynolds equation. The difference between the two calculated film shapes is used to iterate the actual pressure field, that is, the pressure is adjusted until the two shapes agree with each other. This iteration procedure typically fails when the film thickness becomes too small or the pressure is too high. In this regime, convergence can be very slow and can involve many iterations. A common way to alleviate these difficulties is to use the inverse solution method first introduced by (Dowson and Higginson, 1959). In this method, direct iteration is applied only in the low-pressure domain and the pressure is solved inversely in the high-pressure region. This method is found to be successful in handling high pressures. For example, (Lee and Cheng, 1973) have obtained the pressure and deformation profiles between two normally approaching lubricated cylinders using direct iteration in the low pressure (inlet) region and using Newton-Raphson to solve the nonlinear equation in the high-pressure region. However, this procedure often requires manual adjustments, and the region of high/low pressure could change continuously depending on the loading history. As a result, this method is not fully automatic. Likewise, in the point contact sphere collision problem, Davis reported that their iterative procedure breaks down when the elastic displacement of the colliding spheres is comparable to the initial film thickness (Davis et al., 1986). In their case, convergence in this regime was obtained using a relaxation technique. The relaxation method was first introduced by Hamrock and Dowson to study point EHL contact problems (Hamrock and Dowson, 1976a, 1976b). Again, this procedure usually requires manual adjustment of the relaxation parameters. Recently, a new iterative numerical technique was used by (Wang et al., 2017) to study the deformation of elastic coatings under stationary normal lubricated contact. In this scheme, the thickness of the liquid film is used as the iterant. Once the thickness is specified, the pressure is computed by solving the Reynolds equation. The force acting on the indenter and the elastic displacement are then determined using this pressure. From this displacement one can update the film thickness. The film thickness is iterated until force balance is satisfied.

Although widely used in EHL problems (Ai and Yu, 1988, 1989; Hamrock and Dowson, 1976b; Wu et al., 2020, 2022a) due to its ease of implementation and relatively light computational resource needs, the relaxation method has inherent numerical instabilities for general EHL problems. Additionally, in the transient EHL problem, more than one relaxation parameter is needed (Hui et al., 2021). This makes the selection of the relaxation parameters very difficult, to be carried out by trial and error. Failing to choose proper relaxation parameters results in numerical divergence when solving the coupled Reynolds and elasticity equations under force balance conditions. Since the relaxation factors usually vary from problem to problem, it is also difficult to transfer the learning of the relaxation parameter selection from one study to another. In addition to the relaxation method, there are also other iteration techniques such as the multigrid method which iterates the intermediate solutions of Reynolds and elasticity equations between coarse and fine grids (Brandt and Lubrecht, 1990). More recently, FEM which fully coupled the Reynold's equation and elasticity has been applied to solve EHL problems. However, we note that FEM methods face the same numerical issues, the necessity to iterate and spurious instabilities associated with large loads. For example, (Stupkiewicz, 2009) developed a fully-coupled finite element formulation for steady-state problems and found that the formulation was susceptible to spurious instability and oscillations. Similarly, (Habchi et al., 2012) presented a coupled finite element method which, however, also requires special attention to handle spurious oscillations. These papers focused on steady sliding problems. Even though the basic numerical techniques for transient normal indentation and transient sliding and steady sliding problems are similar, there is no unified method to solve both types of problems in a single operation. This motivates us to develop a more general numerical scheme which is able to solve different EHL problems such as transient normal indentation, steady-state sliding and transient sliding without iteration.

In addition to numerical studies of the contact mechanics in the EHL regime, here we also mention some closely related theoretical and experimental studies. For example, (Sekimoto and Leibler, 1993) proposed a mechanism for non-contact repulsive interaction between elastic bodies lubricated by a thin fluid film. (Skotheim and Mahadevan, 2005) modeled the lubrication of fluid-immersed soft interfaces and showed that elastic deformation couples tangential and normal forces and thus generates lift. (Leroy and Charlaix, 2011) showed that forcing oscillatory flows of confined liquid in elasto-hydrodynamic interaction provides a unique method to determine the elastic properties of the supported soft layers. (Villey et al., 2013) studied the rheology of nanometric liquids and found that the elastic deformation of confining surfaces must be taken into account when calculating the hydrodynamic impedance; (Snoeijer et al., 2013) studied lubricated sliding of a rigid cylinder under Hertz-like conditions and proposed a useful scaling for the fluid thickness in the Hertz-like limit; (Chandler and Vella, 2020) studied the lubricated sliding and rolling of a rigid cylinder on a Winkler foundation. (Kargar-Estahbanati and Rallabandi, 2021) studied the lift forces on three-dimensional elastic and viscoelastic lubricated contacts and used the Lorentz reciprocal theorem to directly link the lift force with the underlying linear response function of the bulk material. In a recent study, (Zhang et al., 2020) directly measured the elastohydrodynamic lift force at the nanoscale using atomic force miscroscopy, and their results were in a good agreement with scaling arguments and a quantitative model of soft lubrication theory.

In this paper, we propose a novel method to solve the EHL problem without resorting to iteration. The method boils down to solving

a linear system of equations at each time step. The numerical scheme is stable and can be implemented using standard matrix solvers such as those found in MATLAB (The MathWorks, 2020). The solution scheme is fully automatic and can be applied to transient problems. We demonstrated this technique by studying a fundamental problem: the *transient* contact mechanics of a rigid sphere on a lubricated elastic half space under time dependent normal and shear loads. The plan of the remainder of the paper is as follows: Section 2 gives the governing equations for a point contact problem which works for both normal indention and sliding. The numerical method is presented in section 3 and we use it to solve a point contact problem in which the sphere first undergoes normal contact, followed by transient sliding, that then reaches steady state. Section 4 validates our numerical method by solving the problem of a rigid cylinder undergoing transient sliding on an elastic foundation. We conclude in Section 5 and discuss the superiority and the potential applications of this new numerical method, specially to transient soft-EHL problems.

# 2. Governing equations for a rigid sphere in lubricated contact with an elastic half space

Figure 1 shows the geometry. Material points of the elastic substrate occupy the half space Z < 0. Here (X, Y, Z) is a Cartesian coordinate system fixed in space. The rigid sphere, of radius R, is sliding with velocity V(t) in X direction relative to the half space, where t is time. Without loss in generality, we assume  $t \ge 0$  and V(t = 0) = 0. Note  $h_c(t = 0) > 0$  is the initial liquid layer thickness at the tip of the sphere (X = Y = 0) and V(X = 0) = 0. So is the vertical elastic displacement of the elastic half space caused by the hydrodynamic pressure V(X,Y,t). For lubrication problem, since the hydrodynamic pressure is dominant over viscous shear, the horizontal displacement is neglected. Although the Reynolds equation can be written with respect to the stationary frame, it is more convenient to rewrite the equation in a moving frame V(X,Y,t) that is attached to the sphere. The two coordinate systems are related by

$$x = X - D(t), y = Y, z = Z \text{ where } D(t) \equiv \int_{0}^{t} V(t')dt'$$
(1)

is the horizontal distance travelled by the sphere at time t. With respect to this moving coordinate system, the Reynolds equation is (see SI):

$$\left(\frac{p_{,x}d^3}{12\eta}\right)_{,x} + \left(\frac{p_{,y}d^3}{12\eta}\right)_{,y} = -\left(\frac{V(t)}{2}\right)d_{,x} + d_{,t}$$
 (2a)

where  $\eta$  is the liquid viscosity, the comma denotes partial derivative, i.e.,  $\partial(\bullet)/\partial x = (\bullet)_{,x}$  etc., p(x,y,t) is the hydrodynamic pressure, and

$$d \equiv h - w, \tag{2b}$$

is the thickness of the liquid layer defined in the moving frame and

$$h = h_c(t) - \frac{x^2 + y^2}{2R},$$
 (2c)

is the position of the sphere surface relative to the undeformed flat surface of the substrate, (see Fig. 1). The vertical elastic displacement w = w(x, y, t) is related to p by (Johnson, 1985):

$$w(x,y) = -\frac{1}{4\pi G} \int_{-\infty}^{\infty} \int_{-\infty}^{\infty} \frac{p(x',y')dx'dy'}{\sqrt{(x-x')^2 + (y-y')^2}}$$
(3)

where G is the shear modulus of the substrate, which we assume to be incompressible, which is a good assumption for most soft materials. For compressible solids with Poisson's ratio  $\nu$ , one merely replaces 1/G in (3) by  $2(1-\nu)/G$ . Equations (2a-c) and (3) are the governing equations. These equations can be easily modified to study transient sliding of a cylinder (see derivation and the validation example in SI).

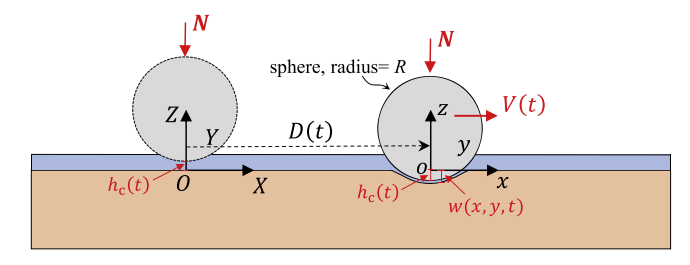


Fig. 1. A schematic of a rigid sphere in lubricated contact with an elastic half space. Normal contact when sliding velocity V=0. Sliding contact occurs when V>0.

The advantage of Eq. (2a) can be illustrated by considering a situation typically encountered in experiments (see Fig. 2): At time t = 0, the sphere is moved downwards at a constant rate  $\dot{h}$  and with no sideway motion, i.e.,

$$h_c(t) = h_0 - ht$$
,  $0 < t < t_1$  (4a)

$$V(t_1 > t \ge 0) = 0 \Leftrightarrow D(t_1 > t \ge 0) = 0$$
 (4b)

where  $h_c(t=0) \equiv h_0$ . For the case  $0 \le t \le t_1$  the indenter has no sideway motion, i.e. D=0 and x=X,y=Y,z=Z. Next, at  $t>t_1$ , we fix the vertical position of the sphere so that  $h_c(t>t_1)=h_0-\dot{h}t_1\equiv -h_\infty$  (here we assume indentation is large enough so  $h_\infty$  is positive) and then impose a sliding velocity  $V(t>t_1)>0$  to the sphere. For example, one can prescribe the following velocity history:

$$V(t) = \begin{cases} 0, & t < t_1 \\ V_{ss} \tanh\left(\frac{t - t_1}{T}\right), & t \ge t_1 \end{cases} \Rightarrow D(t) = \begin{cases} 0, & t < t_1 \\ V_{ss} T \ln\left(\cosh\left(\frac{t - t_1}{T}\right)\right), & t \ge t_1 \end{cases}$$
 (5)

where T is a characteristic loading time to be specified. Note since the tanh function approaches 1 rapidly for  $t - t_1 \ge T$ , we expect that for  $t >> t_1 + T$ , the transient solution should converge to the steady state sliding solution (with velocity  $V_{ss}$ ). This example illustrates that the present formulation can solve realistic transient problems. In addition, it also provides a simple method to determine steady state solutions, thus avoiding the need to develop separate numerical methods for transient and steady sliding problems.

In the following, we will use our newly developed numerical method to simulate the transient sliding of a rigid sphere with loading history described by Eqs. (4a,b) and Eq. (5) above (see Fig. 2). The final results will be validated using the steady state solution shown in (Wu et al., 2020).

# 3. A unified numerical method to solve EHL problems

In this example, we solve the complex transient problem described earlier by Eqs. (4a,b) and (5). Briefly, the loading history consists of three steps: transient normal indentation (TNI), transient sliding (TS), which goes to steady-state sliding (SS). The history of the sphere's horizontal translating velocity  $V(\bar{t})$ , vertical indentation depth  $\bar{h}_0(\bar{t})$  are shown in the Fig. 2 (see also Eqs. (4a,b) and (5)).

Note that the solution is not axisymmetric during the sliding phase; however, it is still useful to use a cylindrical coordinate system  $(r, \theta, z)$ ; then Eqs. (2a) and (3) are replaced by (Wu et al., 2020)

$$\frac{1}{r}\frac{\partial}{\partial r}\left(\frac{1}{12\eta}r\frac{\partial p}{\partial r}\cdot d^3\right) + \frac{1}{r}\frac{\partial}{\partial \theta}\left(\frac{1}{12\eta}\frac{1}{r}\frac{\partial p}{\partial \theta}\cdot d^3\right) = -\frac{V(t)}{2}\left(\cos\theta\frac{\partial d}{\partial r} - \frac{\sin\theta}{r}\frac{\partial d}{\partial \theta}\right) + \frac{\partial d}{\partial t}$$
(6)

$$w(r,\theta) = -\frac{1}{4\pi G} \int_{0}^{2\pi} \int_{0}^{\infty} \frac{p(r',\theta')r'dr'd\theta'}{\sqrt{(r\cos\theta - r'\cos\theta')^2 + (r\sin\theta - r'\sin\theta')^2}}$$
(7)

The use of a cylindrical coordinate system reduces the number of elements in the finite difference mesh since the fluid pressure varies slowly in the  $\theta$  direction. We introduce the following normalization:

$$\bar{r} = \frac{r}{\sqrt{Rh_{\infty}}}, \bar{t} = \frac{V_{ss}t}{2\sqrt{Rh_{\infty}}}, \ \bar{w} = \frac{w}{h_{\infty}}, \ \bar{h} = \frac{h}{h_{\infty}}, \ \bar{d} = \frac{d}{h_{\infty}}, \ \bar{p} = \frac{p}{4\pi G \sqrt{h_{\infty}/R}}, \tag{8a-g}$$

This normalization is motivated by the classical result of Hertz contact theory where the contact radius  $a_H$  is given by  $a_H = \sqrt{Rh_\infty}$  (Johnson, 1985). Recall that the Hertz pressure distribution  $p_H$  is axisymmetric and is given by

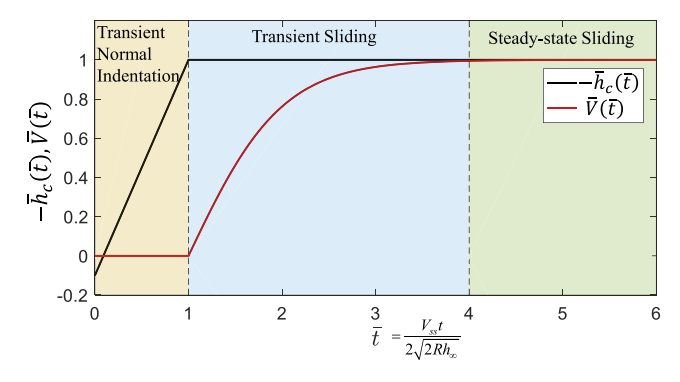


**Fig. 2.** A loading history consisting of a transient normal indentation process (V = 0), a transient sliding phase (V > 0) and a steady-state sliding phase  $\overline{V} = V/V_{ss} = 1$  (see Eqs. (4) and (5));

$$p_H(r) = \begin{cases} (8G/\pi)\sqrt{h_\infty/R}\sqrt{1 - (r^2/Rh_\infty)}, & r \le \sqrt{Rh_\infty} \\ 0, & r > \sqrt{Rh_\infty} \end{cases}$$

$$(9)$$

The normalized forms of Eqs. (6) and (7) are

$$\frac{\beta}{\overline{r}}\frac{\partial}{\partial \overline{r}}\left(\overline{r}\frac{\partial \overline{p}}{\partial \overline{r}}\cdot\overline{d}^{3}\right) + \frac{\beta}{\overline{r}}\frac{\partial}{\partial \theta}\left(\frac{1}{\overline{r}}\frac{\partial \overline{p}}{\partial \theta}\cdot\overline{d}^{3}\right) = -\overline{V}(\overline{t})\left(\cos\theta\frac{\partial\overline{d}}{\partial \overline{r}} - \frac{\sin\theta}{\overline{r}}\frac{\partial\overline{d}}{\partial \theta}\right) + \frac{\partial\overline{d}}{\partial \overline{t}}$$
(10a)

$$\overline{w} = -\int_{0}^{2\pi} \int_{0}^{\infty} \frac{\overline{p}(\overline{r'}, \theta') \overline{r'} d\overline{r'} d\theta'}{\sqrt{(\overline{r}\cos\theta - \overline{r'}\cos\theta')^2 + (\overline{r}\sin\theta - \overline{r'}\sin\theta')^2}}$$
(10b)

where

$$\overline{d} = \overline{h} - \overline{w}, \ \overline{h} = \begin{cases}
\frac{h_0}{h_\infty} - \frac{\dot{h}}{h_\infty} \frac{2\sqrt{Rh_\infty}}{V_{ss}} \overline{t} + \overline{r}^2 / 2, & \overline{t} \le \frac{V_{ss}t_1}{2\sqrt{Rh_\infty}} = \frac{V_{ss}}{2\sqrt{Rh_\infty}} \frac{h_0 + h_\infty}{\dot{h}} \equiv \overline{t}_1 \\
-1 + \overline{r}^2 / 2, & \overline{t} \le \frac{V_{ss}t_1}{2\sqrt{Rh_\infty}} = \frac{V_{ss}}{2\sqrt{Rh_\infty}} \frac{h_0 + h_\infty}{\dot{h}} \equiv \overline{t}_1
\end{cases} \tag{10c}$$

$$\overline{V}(\overline{t}) = \begin{cases} 0, & \overline{t} < \overline{t}_1 \\ & \tanh\left(\frac{2\sqrt{Rh_{\infty}}}{V_{ss}t_1}\overline{t} - 1\right), & \overline{t} \ge \overline{t}_1 \end{cases}$$
 (10d)

and $\beta$ is a dimensionless parameter defined by

$$\beta = \frac{2}{3} \frac{h_{\infty}^2}{R} \frac{\pi G}{\eta V_{\text{vs}}}.$$
 (10e)

Note that, for convenience, we have chosen  $T = t_1$  in Eq. (5). In the following, we choose

$$\frac{\dot{h}}{h_0 + h_\infty} \frac{2\sqrt{Rh_\infty}}{V_{ext}} = 1 \text{ and } \frac{2\sqrt{Rh_\infty}}{V_{ext}} = 1$$
(11)

The choice specified by Eq. (11) reduces the number of parameters in the simulation and does not affect the viability of the numerical scheme. Using Eq. (11), Eq. (10c,d) becomes:

$$\bar{h} = \begin{cases}
\frac{h_0}{h_\infty} - \left(1 + \frac{h_0}{h_\infty}\right)\bar{t} + \bar{r}^2 / 2, & \bar{t} \le 1 \\
-1 + \bar{r}^2 / 2, & \bar{t} > 1
\end{cases}$$
(12a)

$$\overline{d} = \begin{cases} \frac{h_0}{h_{\infty}} - \left(1 + \frac{h_0}{h_{\infty}}\right)\overline{t} + \overline{r}^2 / 2 - \overline{w}, & \overline{t} \le 1\\ -1 + \overline{r}^2 / 2 - \overline{w}, & \overline{t} > 1 \end{cases}$$
(12b)

$$\overline{V}(\overline{t}) = \begin{cases} 0, & \overline{t} < 1\\ \tanh(\overline{t} - 1), & \overline{t} \ge 1 \end{cases}$$
 (12c)

This simplification reduces the number of parameters to 2; these are  $\beta$  and  $\frac{h_0}{h_\infty}$ . We note that the dimensionless parameter  $\beta$  plays a dual role in our calculation. First,  $1/\beta$  represents the normalized velocity in the steady state sliding problem. Second, due to Eq. (11),  $1/\beta$  represents the normalized loading rate before sliding occur.

# 3.1. Numerical method: Reynolds equation

In this section we present the details of our numerical method to solve the nonlinear Reynolds equation. Equation (10a) can be rewritten as:

$$\beta \left[ \frac{\partial \overline{p}}{\partial \overline{r}} \cdot N(\overline{r}, \theta, \overline{t}) + \frac{\partial^2 \overline{p}}{\partial \overline{r}^2} \cdot \overline{d}^3 + \frac{1}{\overline{r}^2} \left( \frac{\partial^2 \overline{p}}{\partial \theta^2} \cdot \overline{d}^3 + M(\overline{r}, \theta, \overline{t}) \frac{\partial \overline{p}}{\partial \theta} \right) \right] = -\overline{V}(\overline{t}) \left( \cos \theta \frac{\partial \overline{d}}{\partial \overline{r}} - \frac{\sin \theta}{\overline{r}} \frac{\partial \overline{d}}{\partial \theta} \right) + \frac{\partial \overline{d}}{\partial \overline{t}}$$

$$(13a)$$

where

$$N(\overline{r},\theta,\overline{t}) \equiv \overline{d}^2 \left( \frac{\overline{d}}{\overline{r}} + 3 \frac{\partial \overline{d}}{\partial \overline{r}} \right), \ M(\overline{r},\theta,\overline{t}) \equiv 3 \overline{d}^2 \frac{\partial \overline{d}}{\partial \theta}$$
 (13b)

$$\frac{\partial \overline{d}}{\partial \overline{r}} = \overline{r} - \frac{\partial \overline{w}}{\partial \overline{r}}, \quad \frac{\partial \overline{d}}{\partial \theta} = -\frac{\partial \overline{w}}{\partial \theta}, \quad \frac{\partial \overline{d}}{\partial \overline{t}} = \begin{cases}
-\left(1 + \frac{h_0}{h_\infty}\right) - \frac{\partial \overline{w}}{\partial \overline{t}}, & \overline{t} \leq 1 \\
-\frac{\partial \overline{w}}{\partial \overline{t}}, & \overline{t} > 1
\end{cases}$$
(13c)

The pressure and displacement are even functions of  $\theta$ , hence only $\Omega = [0, \pi] \times [0, \overline{L}]$  is used. The calculation domain and the boundary conditions are shown in the Fig. 3.

We use a uniform mesh in both the radial and  $\theta$  direction (see Fig. 3), i.e.,

$$\bar{r}_{i+1} = \bar{r}_i + \Delta \bar{r}, \bar{r}_1 = 0, j = 1, ..., n$$
 (14a)

$$\theta_{i+1} = \theta_i + \Delta\theta, \theta_1 = 0, i = 1, \dots, m. \tag{14b}$$

We use equal time steps, with time at step k at  $t_k = k\Delta t$ , k = 0, 1, ... The pressure and displacement at  $t_k$  are denoted by  $p(\theta_i, r_j, t_k) \equiv p_{ii}^k$ ,  $w(\theta_i, r_i, t_k) \equiv w_{ii}^k$ , respectively.

At time  $t_{k+1}$ , we evaluate all the nonlinear terms  $N(\bar{r}, \theta, \bar{t}) \equiv \overline{d}^2(\frac{\bar{d}}{\bar{r}} + 3\frac{\partial \bar{d}}{\partial \bar{r}})$ ,  $M(\bar{r}, \theta, \bar{t}) \equiv 3\overline{d}^2\frac{\partial \bar{d}}{\partial \bar{\theta}}$  and  $\overline{d}^3$  in the LHS of Eq. (13a) using their values at the previous time step, i.e., at  $t_k$ . Denote  $N(\theta_i, \bar{r}_j, \bar{t}_k) \equiv N_{i,j}^k$ ,  $M(\theta_i, \bar{r}_j, \bar{t}_k) \equiv M_{i,j}^k$  and  $\overline{d}^3(\theta_i, \bar{r}_j, \bar{t}_k) \equiv (\overline{d}_{i,j}^k)^3$ . The numerical scheme for the pressure and displacement at time step k+1 is

$$\beta \left[ \left( \frac{\partial \overline{p}}{\partial \overline{r}} \right)_{i,j}^{k+1} N_{i,j}^{k} + \left( \frac{\partial^{2} \overline{p}}{\partial \overline{r}^{2}} \right)_{i,j}^{k+1} \left( \overline{d}_{i,j}^{k} \right)^{3} + \frac{1}{\overline{r}_{j}^{2}} \left( \left( \frac{\partial^{2} \overline{p}}{\partial \theta^{2}} \right)_{i,j}^{k+1} \left( \overline{d}_{i,j}^{k} \right)^{3} + M_{i,j}^{k} \left( \frac{\partial \overline{p}}{\partial \theta} \right)_{i,j}^{k+1} \right) \right] \\
= -\overline{V}(\overline{t}_{k+1}) \left( \cos\theta \left( \overline{r}_{j} - \left( \frac{\partial \overline{w}}{\partial \overline{r}} \right)_{i,j}^{k+1} \right) + \frac{\sin\theta}{\overline{r}_{j}} \left( \frac{\partial \overline{w}}{\partial \theta} \right)_{i,j}^{k+1} \right) + \left( \frac{\partial d}{\partial t} \right)_{i,j}^{k+1} \qquad (1 < i < m, \ 1 < j < n) \right)$$

where:

$$\overline{V}(\overline{t}_{k+1}) = \begin{cases} 0, & \overline{t}_{k+1} < 1 \\ & \tanh(\overline{t}_{k+1} - 1), & \overline{t}_{k+1} \ge 1 \end{cases}; \quad \left(\frac{\partial d}{\partial t}\right)_{i,j}^{k+1} = \begin{cases} -\left(1 + \frac{h_0}{h_\infty}\right) - \left(\frac{\partial \overline{w}}{\partial \overline{t}}\right)_{i,j}^{k+1}, & \overline{t}_{k+1} \le 1 \\ -\left(\frac{\partial \overline{w}}{\partial \overline{t}}\right)_{i,j}^{k+1}, & \overline{t}_{k+1} > 1 \end{cases}$$

$$(16a,b)$$

Note that j > 1 in Eq. (15) so  $\bar{r}_1 = 0$  presents no difficulty. To deal with the singularity due to the use of cylindrical coordinates at  $\bar{r} = 0$ , we use the condition  $\frac{\partial \bar{p}}{\partial \bar{r}}|_{\bar{r}=0} = 0$ , which is:

$$\vec{p}_{i,i=1}^k = \vec{p}_{i,i=2}^k.$$
 (17a)

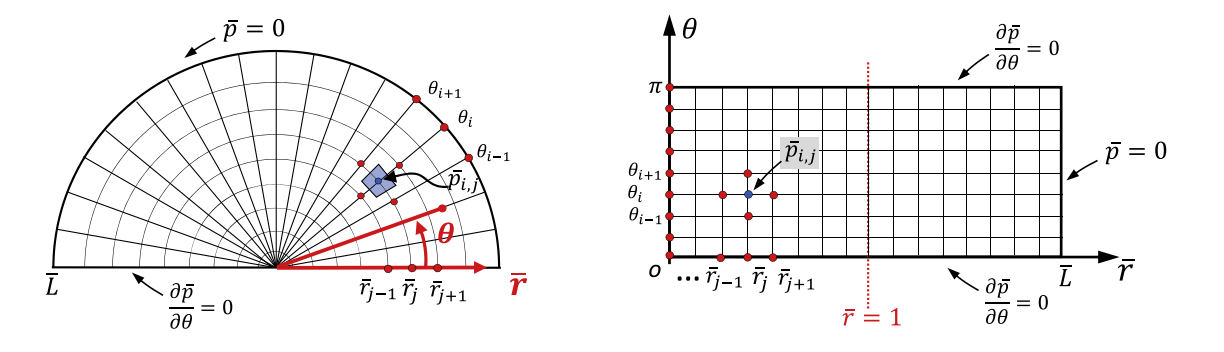


Fig. 3. A schematic of the calculation domain, the finite difference mesh and the boundary conditions.

On the boundary  $\theta = 0$  and  $\theta = \pi$ , reflective symmetry requires  $\frac{\partial \overline{p}}{\partial \theta} = 0$ . Therefore:

$$\bar{p}_{i=1,j}^k = \bar{p}_{i=2,i}^k, \ \bar{p}_{i=m,j}^k = \bar{p}_{i=m-1,j}^k$$
(17b)

The boundary condition that pressure vanishes at distances far from the origin is satisfied by

$$\overline{p}_{i,i=n}^k = 0 \tag{18a}$$

The initial condition that pressure vanishes everywhere is:

$$\overline{p}_{i,j}^{k=0} = 0 \tag{18b}$$

We applied standard finite differences for the first and second derivatives at  $\theta = \theta_i, r = r_i$  at time  $t_k$ , that is:

$$\left(\frac{\partial \overline{p}}{\partial \overline{r}}\right)_{ij}^{k} = \frac{\overline{p}_{i,j+1}^{k} - \overline{p}_{i,j}^{k}}{\Delta \overline{r}}, \left(\frac{\partial^{2} \overline{p}}{\partial \overline{r}^{2}}\right)_{ij}^{k} = \frac{\overline{p}_{i,j+1}^{k} - 2\overline{p}_{i,j}^{k} + \overline{p}_{i,j-1}^{k}}{(\Delta \overline{r})^{2}} \\
\left(\frac{\partial \overline{p}}{\partial \theta}\right)_{ii}^{k} = \frac{\overline{p}_{i+1,j}^{k} - \overline{p}_{i,j}^{k}}{\Delta \theta}, \left(\frac{\partial^{2} \overline{p}}{\partial \theta^{2}}\right)_{ij}^{k} = \frac{\overline{p}_{i+1,j}^{k} - 2\overline{p}_{i,j}^{k} + \overline{p}_{i-1,j}^{k}}{(\Delta \theta)^{2}} \right) \tag{19a-d}$$

$$\left(\frac{\partial \overline{w}}{\partial \overline{r}}\right)_{ij}^{k} = \frac{\overline{w}_{i,j+1}^{k} - \overline{w}_{i,j}^{k}}{\Delta \overline{r}}, \left(\frac{\partial \overline{w}}{\partial \theta}\right)_{ij}^{k} = \frac{\overline{w}_{i+1,j}^{k} - \overline{w}_{i,j}^{k}}{\Delta \theta}$$
(19c,d)

The finite difference for the time derivative is:

$$\left(\frac{\partial \overline{w}}{\partial \overline{t}}\right)_{i,i}^{k+1} = \frac{\overline{w}_{i,j}^{k+1} - \overline{w}_{i,j}^{k}}{\Delta \overline{t}}$$
(19e)

Substituting Eq. (19) into Eq. (15) gives:

$$A_{i,j}\overline{p}_{i-1,j}^{k+1} + B_{i,j}\overline{p}_{i,j-1}^{k+1} + C_{i,j}\overline{p}_{i,j}^{k+1} + D_{i,j}\overline{p}_{i,j+1}^{k+1} + E_{i,j}\overline{p}_{i+1,j}^{k+1} + F_{i,j}\overline{p}_{i+1,j}^{k+1} + F_$$

where:

$$A_{i,j} = \frac{\lambda^2}{\overline{r}_j^2} \left(\overline{d}_{i,j}^k\right)^3, \ B_{i,j} = \left(\overline{d}_{i,j}^k\right)^3, \ C_{i,j} = -2\left(\overline{d}_{i,j}^k\right)^3 \left[1 + \frac{\lambda^2}{\overline{r}_j^2}\right] - \left[N_{i,j}^k + \frac{\lambda M_{i,j}^k}{\overline{r}_j^2}\right] \Delta \overline{r}$$

$$D_{i,j} = \left(\overline{d}_{i,j}^k\right)^3 + N_{i,j}^k \Delta \overline{r}, \ E_{i,j} = \frac{1}{\overline{r}_i^2} \left[\lambda^2 \left(\overline{d}_{i,j}^k\right)^3 + \lambda M_{i,j}^k \Delta \overline{r}\right]$$

$$(21a-e)$$

$$F_{i,j} = \beta^{-1} \Delta \overline{r} \cdot \overline{V}(\overline{t}_{k+1}) \left( \cos \theta_i - \frac{\lambda \sin \theta_i}{\overline{r}_j} \right) + \frac{\left( \Delta \overline{r} \right)^2}{\beta \Delta \overline{t}}, \ G_{i,j} = -\beta^{-1} \Delta \overline{r} \cdot \overline{V}(\overline{t}_{k+1}) \cos \theta_i,$$

$$H_{i,j} = eta^{-1} \Delta \overline{r} \cdot \overline{V}(\overline{\imath}_{k+1}) rac{\lambda \sin heta_i}{\overline{r}_i}$$
 (22a-c)

$$f_{i,j} = \begin{cases} -\beta^{-1} (\Delta \overline{r})^2 \left[ \left( 1 + \frac{h_0}{h_\infty} \right) + \overline{r}_j \cdot \overline{V}(\overline{t}_{k+1}) \cos \theta_i \right] + \frac{(\Delta \overline{r})^2}{\beta \Delta \overline{t}} \overline{W}_{i,j}^k, & \overline{t}_{k+1} \le 1 \\ -\beta^{-1} (\Delta \overline{r})^2 \left[ 0 + \overline{r}_j \cdot \overline{V}(\overline{t}_{k+1}) \cos \theta_i \right] + \frac{(\Delta \overline{r})^2}{\beta \Delta \overline{t}} \overline{W}_{i,j}^k, & \overline{t}_{k+1} > 1 \end{cases}$$

$$(23)$$

where  $\lambda \equiv \frac{\Delta \overline{r}}{\Delta \theta}$ . Since the coefficients  $A_{i,j}, B_{i,j}, C_{i,j}, D_{i,j}, E_{i,j}, F_{i,j}, G_{i,j}$  and  $f_{i,j}$  are completely determined at time step k, Eq. (20) is a linear system of equations with  $n \times m$  unknowns  $\overline{p}_{i,j}^{k+1}$  and  $n \times m$  unknowns  $\overline{w}_{i,j}^{k+1}$  at the k+1 time step.

# 3.2. Coupling hydrodynamic pressure to substrate surface displacement

The linearized equation Eq. (20) is coupled to substrate deformation through Eq. (10b), which provides a linear relation relating  $\overline{w}$  to  $\overline{p}$  in the form of a double integral. In a previous work (Wu et al., 2020), we have developed a numerical scheme to discretize this linear relationship at any time step. Here we modified this scheme slightly. We divided the surface into many small quadrilaterals (such as  $\square BCDE$  in Fig. 4). On each of these quadrilaterals the pressure is uniform. For the purpose of illustration, consider point A at  $(\theta_i, \overline{r}_i)$  with the center at the grid point  $(\theta_k, \overline{r}_l)$ .  $\theta_k = (\theta_B + \theta_E)/2$  and  $\overline{r}_l = (\overline{r}_B + \overline{r}_C)/2$  where  $\theta_B$  and  $\theta_E$  are the  $\theta$  coordinate of vertices of B and B;

 $\overline{r}_B$  and  $\overline{r}_C$  are the  $\overline{r}$  coordinate of B and C. The vertical displacement at point A at  $(\theta_i, \overline{r}_j)$  due to the uniform pressure  $\overline{p}_{k,l}$  on the  $\square BCDE$  is denoted by  $\overline{w}_{A, \square BCDE}$  or  $\overline{w}_{(i,j),(k,l)}$ . The calculation of  $\overline{w}_{(i,j),(k,l)}$  has been shown in our previous work (Wu et al., 2020) by decomposing the quadrilateral  $\square BCDE$  into a linear combination of four triangles:  $\square BCDE = -\Delta ACB + \Delta ADC + \Delta ADE - \Delta AEB$  and adding the displacement due to the pressure on each of these triangles, the result is:

$$\overline{w}_{(i,j),(k,l)} \equiv \overline{w}_{A,\square BCDE} = -\overline{w}_{A,\Delta ACB} + \overline{w}_{A,\Delta ACD} + \overline{w}_{A,\Delta ADE} - \overline{w}_{A,\Delta AEB}$$

$$= \frac{\overline{p}_{k,l}}{8\pi G} \begin{cases}
-h_1 \left[ \ln\left(\frac{1+\sin\varphi_{1C}}{1-\sin\varphi_{1C}}\right) - \ln\left(\frac{1+\sin\varphi_{1B}}{1-\sin\varphi_{1B}}\right) \right] + h_2 \left[ \ln\left(\frac{1+\sin\varphi_{2D}}{1-\sin\varphi_{2D}}\right) - \ln\left(\frac{1+\sin\varphi_{2C}}{1-\sin\varphi_{2C}}\right) \right] \\
+h_3 \left[ \ln\left(\frac{1+\sin\varphi_{3D}}{1-\sin\varphi_{3D}}\right) - \ln\left(\frac{1+\sin\varphi_{3E}}{1-\sin\varphi_{3E}}\right) \right] - h_4 \left[ \ln\left(\frac{1+\sin\varphi_{4E}}{1-\sin\varphi_{4E}}\right) - \ln\left(\frac{1+\sin\varphi_{4B}}{1-\sin\varphi_{4B}}\right) \right]$$

$$= x_{ABB} = \overline{0}$$
(24)

The total deformation  $\overline{w}_{ij}$  at the point  $(\theta_i, \overline{r}_j)$  is then obtained by summing the displacement due to the pressure on all the quadrilaterals, i.e.,

$$\overline{w}_{i,j} = \sum_{k=1}^{m} \sum_{l=1}^{n} \overline{w}_{(i,j),(k,l)} = \sum_{k=1}^{m} \sum_{l=1}^{n} \chi_{(i,j),(k,l)} \overline{p}_{k,l}$$
(25)

# 3.3. The EHL linear system

Combining Eqs. (20-23) and Eq. (25), we obtain the full linear system of equations for the transient EHL problem. They can be written as:

$$\begin{bmatrix} \mathbf{K}_{11} & \mathbf{K}_{12} \\ \mathbf{K}_{21} & \mathbf{K}_{22} \end{bmatrix} \begin{bmatrix} \overline{\mathbf{p}} \\ \overline{\mathbf{w}} \end{bmatrix} = \begin{bmatrix} \mathbf{F}_1 \\ \overline{\mathbf{F}}_2 \end{bmatrix}$$
 (26)

The coefficients vectors  $F_1$ ,  $F_2$  and coefficients matrices of  $K_{11}$ ,  $K_{12}$ ,  $K_{21}$ ,  $K_{22}$  are given in the supporting information. The unknown pressure and displacement vectors are:

$$\overline{p} = \left\{ \overline{p}_{1,1}, \overline{p}_{1,2}, \dots, \overline{p}_{1,n}; \overline{p}_{2,1}, \overline{p}_{2,2}, \dots, \overline{p}_{2,n}; \dots \dots; \overline{p}_{m-1,1}, \overline{p}_{m-1,2}, \dots, \overline{p}_{m-1,n}; \overline{p}_{m,1}, \overline{p}_{m,2}, \dots, \overline{p}_{m,n} \right\}^{T}$$
(27a)

$$\overline{\mathbf{w}} = \left\{ \overline{w}_{1,1}, \overline{w}_{1,2}, \cdots, \overline{w}_{1,n} : \overline{w}_{2,1}, \overline{w}_{2,2}, \cdots, \overline{w}_{2,n} : \cdots : \overline{w}_{m-1,1}, \overline{w}_{m-1,2}, \cdots, \overline{w}_{m-1,n} : \overline{w}_{m,1}, \overline{w}_{m,2}, \cdots, \overline{w}_{m,n} \right\}^{T}$$

$$(27b)$$

We solve the linear system Eq. (26) using a standard matrix solver such as those in MATLAB. Specifically, we start from the initial condition specified in Eq. (18b). Then the linear system is solved for  $\bar{p}$  and  $\bar{w}$ at the next time-step. After that, one increments the time, and the process is repeated to implement time-marching. The numerical scheme is stable and is fully automatic and can be applied to any transient or stationary problems. For completeness, we also provide the numerical setup for the imposed normal force case in the

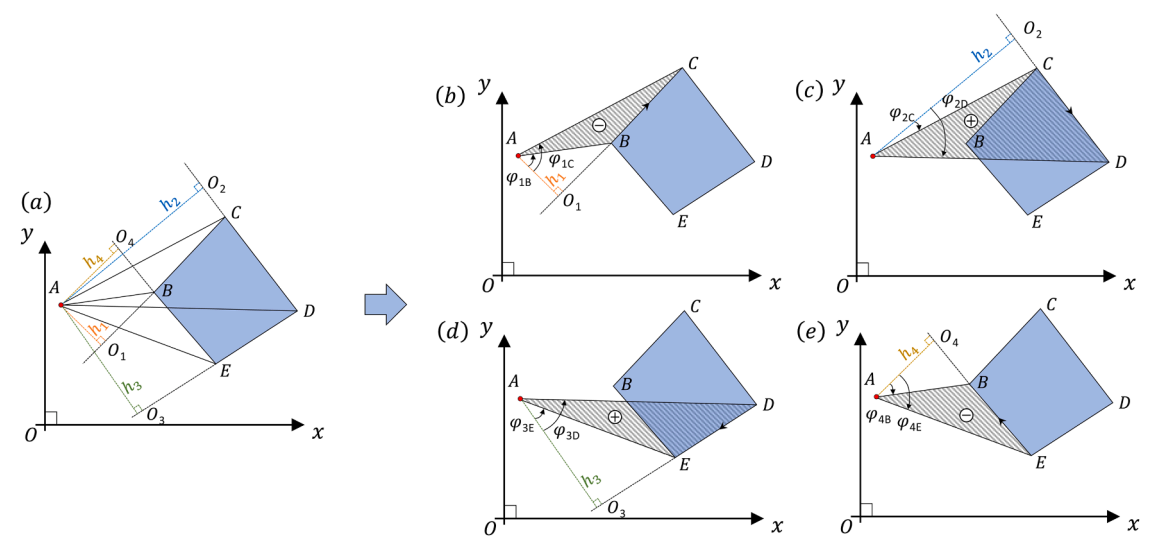


Fig. 4. (a) To calculate the substrate deformation at A point when a uniform pressure is applied at the quadrilateral  $\square BCDE$ ; (b~e) The decomposition of  $\square BCDE$  into 4 triangles  $\triangle ACB$ ,  $\triangle ADC$ ,  $\triangle ADE$ ,  $\triangle AEB$ . The pressure acting on all four triangles are the same and is  $\overline{p}_{k,l}$ .

supporting information.

# 3.4. Numerical results

In the numerical calculation, we fixed the values  $\beta=200$  and  $h_0/h_\infty=-0.1$ . Since  $\beta>>1$ , we expect the solution would be confined at the region of  $\overline{r}\leq 1$ . We choose  $\overline{L}=2$  so the calculation domain  $\Omega=[0,\pi]\times[0,2]$ . The mesh size in  $\overline{r}$  and  $\theta$  direction is dr=0.01,  $d\theta=\pi/60$  respectively. The time increment  $\Delta\overline{t}=0.01$ . we focus on the three different phases of lubricated contact: stationary indentation, transient sliding and steady-state sliding.

# *3.4.1.* Transient Normal Indentation phase $(\bar{t} \le 1)$

In this phase, the sphere moves downwards with no sideway motion, hence all field quantities are axisymmetric. The pressure profile and the fluid thickness profiles at different times are shown in Fig. 5. The hydrodynamic pressure increases with increasing indentation depth  $|h_0|$ . The fluid layer is thinnest at the exit since the fluid velocity is fastest there.

#### 3.4.2. Transition from transient normal indentation to transient sliding $(1 < \overline{t} < 4)$

As indicated by Eq. (5), sliding occur for  $\bar{t} > 1$ . During this phase, the solution is no longer axisymmetric. In particular, as shown in Fig. 6 the pressure peaks at the exit ( $\bar{x} \approx -1$ ), whereas in the s case, the pressure decreases smoothly to zero. Note this peak pressure increases with sliding speed. The larger pressure gradient changes in this region also indicates the fluid exits at a faster rate as sliding speed increases.

# 3.4.3. Steady-state sliding ( $\overline{t} \geq 4$ )

For the long-time case, both the normal indentation and transient sliding has finished. The sphere is expected to be under pure steady-state sliding. The numerical results of  $\beta=200$  at  $\bar{t}=5$  are compared with the steady state solution (obtained using relaxation method (Wu et al., 2020)) as shown in the Fig. 7. The numerical results obtained by directly solving the Eq. (33) at the long time matches the steady solution very well for both pressure and film thickness profile.

The *steady state sliding results* in this work agree well with the similarity solution of (Snoeijer et al., 2013), as shown in our previous work which only considered steady state sliding (Wu et al., 2020). We also noted that the scaling for steady sliding is in agreement with the result of (Zhang et al., 2020). The details are shown in the Supplementary information.

# 4. Further check on new numerical method

Since there is no exact solution for the sphere problem, we check our new numerical method against a simpler problem: a rigid cylinder sliding on an elastic foundation. We choose this problem since an exact *steady state solution* (up to quadrature) is available (Hui et al., 2021) and serves as a check of our numerical method. The agreement between the exact steady state solution based on

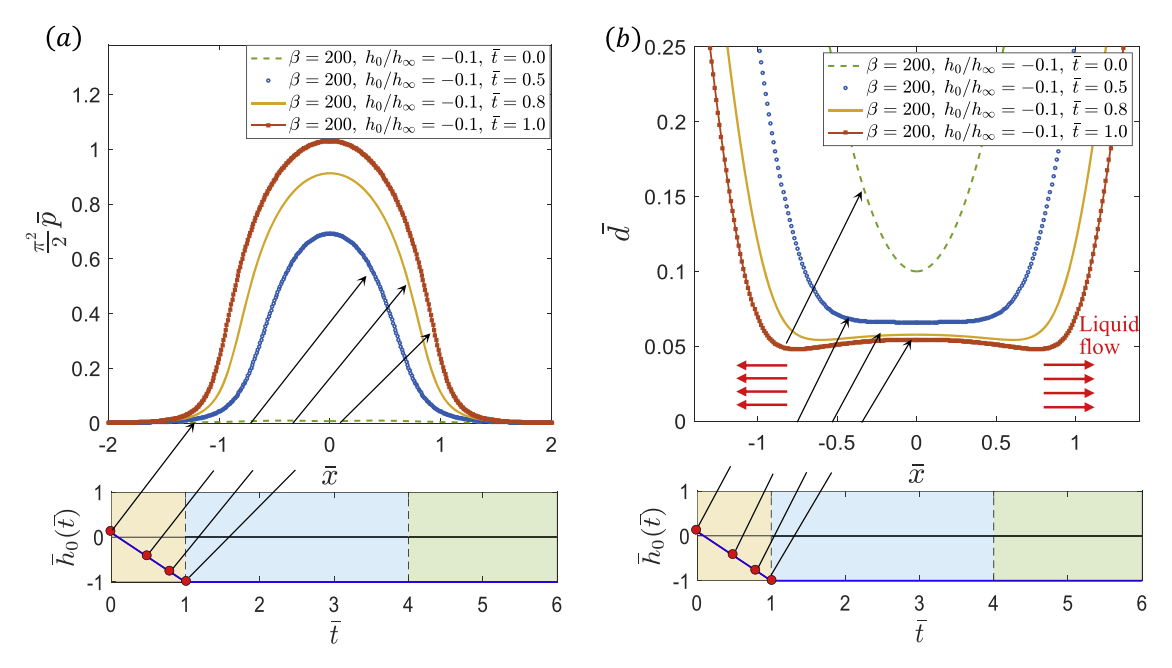
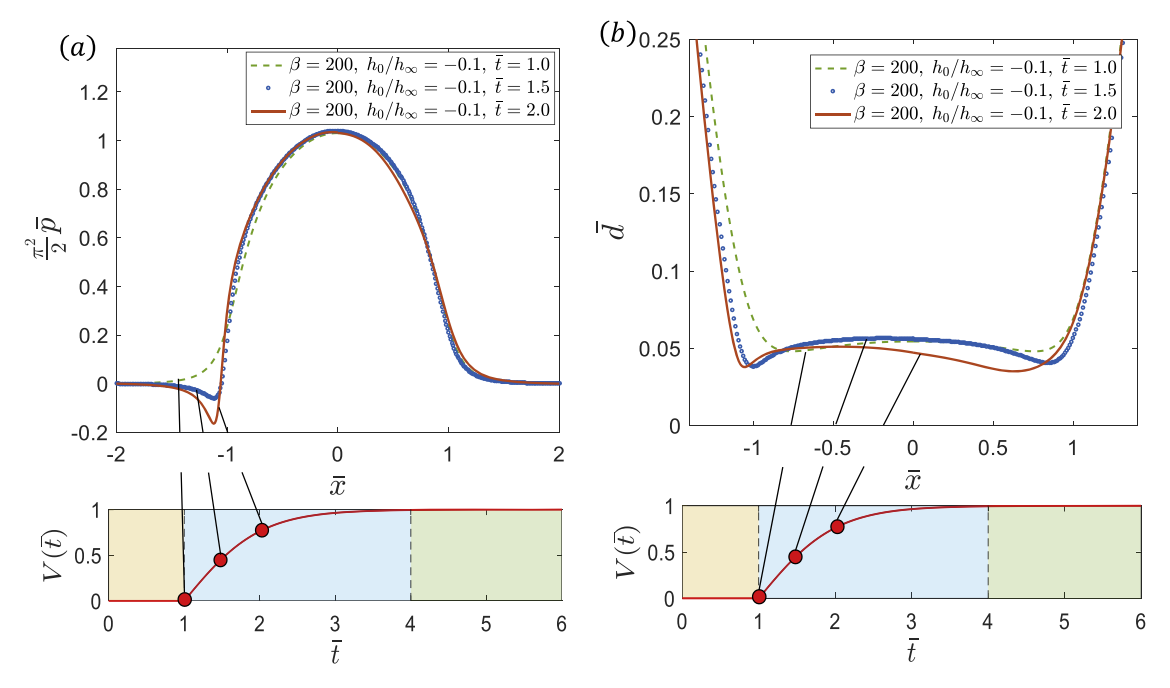


Fig. 5. The hydrodynamic pressure profile and film thickness profile during the transient normal indentation process at different times  $\bar{t} = 0,0.5,0.8,1.0$ . The bottom figures indicate the vertical positions of the sphere as a function of normalized time.



**Fig. 6.** Transition from transient normal indentation to transient sliding at different times  $\bar{t} = 1.0, 1.5, 2.0$ . (a) Pressure profile (b) fluid thickness. The bottom figures indicate the sliding velocity of the sphere as a function of normalized time.

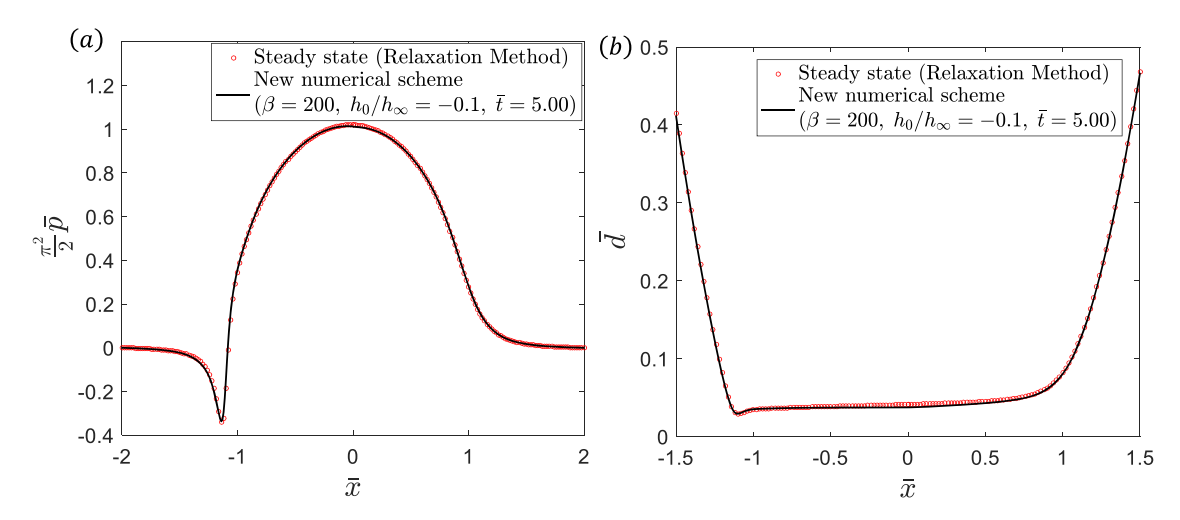


Fig. 7. Comparison of long time solution of our new numerical scheme (solving Eq. (26)) with the steady state solution obtained by the relaxation method (Wu et al., 2020): (a) pressure profile, (b) film thickness profile for  $\beta=200$  and  $h_0/h_\infty=-0.1$ .

quadrature and our numerical method is excellent. Details of implementation and comparison are given in the Supporting information.

#### 5. Summary

The conventional way to solve EHL problems requires iterations of the intermediate solutions between the coupled Reynolds and elasticity equations until all the pressure and displacement fields satisfy both equations and boundary conditions. The stability of these iteration schemes is sensitive to the initial guess of the solution and the iteration parameters such as relaxation factors. Numerical difficulties often occur under high loads or when the elastic displacement is comparable to the film thickness. In addition, conventional solution methods consider normal contact and sliding separately, with much less emphasis given to transient sliding problems.

In this work, we propose a novel numerical scheme to solve the coupled Reynolds and elasticity equations. Our numerical scheme has no iterations and can be fully automated to solve a broad range of EHL problems such as transient normal indentation, transient or steady state sliding. In this paper, we demonstrate this numerical scheme for two EHL problems: Transient lubricated sliding of

cylinder on an elastic foundation, and the transient normal indentation, transient and steady sliding of a point-contact EHL on an elastic half space. The steady state solutions of both cases are validated using established results.

The proposed numerical scheme can be incorporated into homemade and commercial finite element models to solve much more complicated sliding problem such as transient lubricated sliding on structured surfaces. Our numerical method can also be extended to viscoelastic (Carbone and Putignano, 2013; Putignano, 2020; Wu et al., 2022a) or poro-elastic substrates which is important in real applications (Ciapa et al., 2020). Finally, there is no difficulty to including pressure dependent viscosity in our numerical method. We have not included this effect in this work since our focus is on soft materials.

# Declaration of competing interest

The authors declare that they have no known competing financial interests or personal relationships that could have appeared to influence the work reported in this paper.

# **Data Availability**

No data was used for the research described in the article.

# Acknowledgements

The authors acknowledge the support from the National Science Foundation, CMMI-1538002. We also appreciate the suggestions of two anonymous reviewers.

# Supplementary materials

Supplementary material associated with this article can be found, in the online version, at doi:10.1016/j.jmps.2022.105104.

#### References

- Ai, X., Yu, H., 1989. A numerical analysis for the transient EHL process of a Cam-Tappet Pair in I. C. Engine. J. Tribol. 111, 413–417. https://doi.org/10.1115/
- Ai, X., Yu, H., 1988. A full numerical solution for general transient elastohydrodynamic line contacts and its application. Wear 121, 143–159. https://doi.org/10.1016/0043-1648(88)90039-7.
- Bertin, V., Amarouchene, Y., Raphael, E., Salez, T., 2021. Soft-lubrication interactions between a rigid sphere and an elastic wall. arXiv:2104.00900 [cond-mat, physics:physics].
- Brandt, A., Lubrecht, A.A., 1990. Multilevel matrix multiplication and fast solution of integral equations. J. Comput. Phys. 90, 348–370. https://doi.org/10.1016/0021-9991(90)90171-V.
- Carbone, G., Putignano, C., 2013. A novel methodology to predict sliding and rolling friction of viscoelastic materials: theory and experiments. J. Mech. Phys. Solids 61, 1822–1834. https://doi.org/10.1016/j.jmps.2013.03.005.
- Chandler, T.G.J., Vella, D., 2020. Validity of Winkler's mattress model for thin elastomeric layers: beyond Poisson's ratio. Proc Math Phys Eng Sci 476, 20200551. https://doi.org/10.1098/rspa.2020.0551.
- Ciapa, L., Delavoipière, J., Tran, Y., Verneuil, E., Chateauminois, A., 2020. Transient sliding of thin hydrogel films: the role of poroelasticity. Eur. Phys. J. E Soft Matter 16, 6539–6548. https://doi.org/10.1039/D0SM00641F.
- Davis, R.H., 1984. The rate of coagulation of a dilute polydisperse system of sedimenting spheres. J. Fluid Mech. 145, 179. https://doi.org/10.1017/S002211208400286X.
- Davis, R.H., Serayssol, J.-M., Hinch, E.J., 1986. The elastohydrodynamic collision of two spheres. J. Fluid Mech. 163, 479–497. https://doi.org/10.1017/S0022112086002392.
- D'Ottavio, T., Goren, S.L., 1982. Aerosol capture in granular beds in the impaction dominated regime. Aerosol Sci. Technol. 2, 91–108. https://doi.org/10.1080/02786828308958616.
- Dowson, D., Higginson, G.R., 1959. A numerical solution to the elasto-hydrodynamic problem. J. Mech. Eng. Sci. 1, 6–15. https://doi.org/10.1243/JMES\_JOUR\_1959\_001\_004\_02.
- Dowson, D., Jin, Z.-M., 1986. Micro-elastohydrodynamic lubrication of synovial joints. Eng. Med. 15, 63–65. https://doi.org/10.1243/EMED\_JOUR\_1986\_015\_019\_
- Esmen, N.A., Ziegler, P., Whitfield, R., 1978. The adhesion of particles upon impaction. J. Aerosol Sci. 9, 547–556. https://doi.org/10.1016/0021-8502(78)90020-4. Essink, M.H., Pandey, A., Karpitschka, S., Venner, C.H., Snoeijer, J.H., 2021. Regimes of soft lubrication. J. Fluid Mech. 915, A49. https://doi.org/10.1017/ifm.2021.96.
- Evans, H.P., 1981. Inverse Solution of Reynolds' equation of lubrication under point-contact elastohydrodynamic conditions. J. Tribol. 103, 539. https://doi.org/10.1115/1.3251733.
- Habchi, W., Eyheramendy, D., Vergne, P., Morales-Espejel, G., 2012. Stabilized fully-coupled finite elements for elastohydrodynamic lubrication problems. Adv. Eng. Softw. 46, 4–18. https://doi.org/10.1016/j.advengsoft.2010.09.010.
- Hamrock, B.J., Dowson, D., 1976a. Isothermal elastohydrodynamic lubrication of point contacts: part 1—theoretical formulation. J. Lubr. Technol. 98, 223. https://doi.org/10.1115/1.3452801.
- Hamrock, B.J., Dowson, D., 1976b. Isothermal elastohydrodynamic lubrication of point contacts: Part II—Ellipticity parameter results. J. Lubr. Technol. 98, 375. https://doi.org/10.1115/1.3452861.
- Herrebrugh, K., 1970. Elastohydrodynamic squeeze films between two cylinders in normal approach. J. Lubr. Technol. 92, 292–301. https://doi.org/10.1115/1.3451394.
- Hui, C.-Y., Wu, H., Jagota, A., Khripin, C., 2021. Friction force during lubricated steady sliding of a rigid cylinder on a viscoelastic substrate. Tribol. Lett. 69, 30. https://doi.org/10.1007/s11249-020-01396-5.

- Hutt, W., Persson, B.N.J., 2016. Soft matter dynamics: accelerated fluid squeeze-out during slip. J. Chem. Phys. 144, 124903 https://doi.org/10.1063/1.4944384. Jin, Z.M., Dowson, D., 2005. Elastohydrodynamic lubrication in biological systems. Proc. Inst. Mech. Eng. Part J J. Eng. Tribol. 219, 367–380. https://doi.org/10.1243/135065005X33982.
- Johnson, K.L., 1985, Contact Mechanics. Cambridge University Press, Cambridge. https://doi.org/10.1017/CB09781139171731.
- Kargar-Estahbanati, A., Rallabandi, B., 2021. Lift forces on three-dimensional elastic and viscoelastic lubricated contacts. Phys. Rev. E: Stat. Phys., Plasmas, Fluids, Relat. Interdiscip. Top. 6, 034003 https://doi.org/10.1103/PhysRevFluids.6.034003.
- Lee, K.M., Cheng, H.S., 1973. The pressure and deformation profiles between two normally approaching lubricated cylinders. J. Lubr. Technol. 95, 308–317. https://doi.org/10.1115/1.3451813.
- Leroy, S., Charlaix, E., 2011. Hydrodynamic interactions for the measurement of thin film elastic properties. J. Fluid Mech. 674, 389–407. https://doi.org/10.1017/ S0022112010006555
- Li, K.W., Wu, H.H., Lin, Y.-C., 2006. The effect of shoe sole tread groove depth on the friction coefficient with different tread groove widths, floors and contaminants. Appl. Ergon. 37, 743–748. https://doi.org/10.1016/j.apergo.2005.11.007.
- Martz, B.L.S., 1947. Preliminary report of developments in interrupted surface finishes. Proc. Inst. Mech. Eng. 16, 1–9. https://doi.org/10.1111/j.1559-3584.1950. tb02844.x.
- Mcgeehan, J.A., 1978. A literature review of the effects of piston and ring friction and lubricating oil viscosity on fuel economy. In: SAE Technical Paper Series. https://doi.org/10.4271/780673.
- Mourier, L., Mazuyer, D., Lubrecht, A.A., Donnet, C., 2006. Transient increase of film thickness in micro-textured EHL contacts. Tribol. Int. 39, 1745–1756. https://doi.org/10.1016/j.triboint.2006.02.037.
- Moyle, N., Dong, H., Wu, H., Khripin, C.Y., Hui, C.-Y., Jagota, A., 2022. Increased sliding friction of a lubricated soft solid using an embedded structure. Tribol. Lett. 70, 2. https://doi.org/10.1007/s11249-021-01540-9.
- Moyle, N., He, Z., Wu, H., Hui, C.-Y., Jagota, A., 2018. Indentation versus rolling: dependence of adhesion on contact geometry for biomimetic structures. Langmuir 34, 3827–3837. https://doi.org/10.1021/acs.langmuir.8b00084.
- Moyle, N., Wu, H., Khripin, C., Bremond, F., Hui, C.-Y., Jagota, A., 2020. Enhancement of elastohydrodynamic friction by elastic hysteresis in a periodic structure. Eur. Phys. J. E Soft Matter. https://doi.org/10.1039/C9SM02087J, 10.1039.C9SM02087J.
- Okrent, E.H., 1961. The effect of lubricant viscosity and composition on engine friction and bearing wear. ASLE Trans. 4, 97–108. https://doi.org/10.1080/05698196108972423.
- Putignano, C., 2020. Soft lubrication: a generalized numerical methodology. J. Mech. Phys. Solids 134, 103748. https://doi.org/10.1016/j.jmps.2019.103748. Rivetti, M., Bertin, V., Salez, T., Hui, C.-Y., Linne, C., Arutkin, M., Wu, H., Raphaël, E., Bäumchen, O., 2017. Elastocapillary levelling of thin viscous films on soft
- substrates. Phys. Rev. E: Stat. Phys., Plasmas, Fluids, Relat. Interdiscip. Top. 2, 094001 https://doi.org/10.1103/PhysRevFluids.2.094001.

  Saintyves, B., Jules, T., Salez, T., Mahadevan, L., 2016. Self-sustained lift and low friction via soft lubrication. Proc. Natl. Acad. Sci. USA. 113, 5847–5849. https://doi.org/10.1073/pnas.1525462113.
- Sekimoto, K., Leibler, L., 1993. A mechanism for shear thickening of polymer-bearing surfaces: elasto-hydrodynamic coupling. Europhys. Lett. 23, 113–117. https://doi.org/10.1209/0295-5075/23/2/006.
- Skotheim, J.M., Mahadevan, L., 2005. Soft lubrication: the elastohydrodynamics of nonconforming and conforming contacts. Phys. Fluids 17, 092101. https://doi.org/10.1063/1.1985467.
- Snoeijer, J.H., Eggers, J., Venner, C.H., 2013. Similarity theory of lubricated Hertzian contacts. Phys. Fluids 25, 101705. https://doi.org/10.1063/1.4826981. Stupkiewicz, S., 2009. Finite element treatment of soft elastohydrodynamic lubrication problems in the finite deformation regime. Comput. Mech. 44, 605–619. https://doi.org/10.1007/s00466-009-0394-3.
- Touche, T., Cayer-Barrioz, J., Mazuyer, D., 2016. Friction of textured surfaces in EHL and mixed lubrication: effect of the groove topography. Tribol. Lett. 63, 25. https://doi.org/10.1007/s11249-016-0713-8.
- Tzeng, S.T., Saibel, E., 1967. Surface roughness effect on slider bearing lubrication. ASLE Transactions 10, 334–348. https://doi.org/10.1080/05698196708972191. Villey, R., Martinot, E., Cottin-Bizonne, C., Phaner-Goutorbe, M., Léger, L., Restagno, F., Charlaix, E., 2013. Effect of surface elasticity on the rheology of nanometric liquids. Phys. Rev. Lett. 111, 215701 https://doi.org/10.1103/PhysRevLett.111.215701.
- Wang, Y., Tan, M.R., Frechette, J., 2017. Elastic deformation of soft coatings due to lubrication forces. Eur. Phys. J. E Soft Matter 13, 6718–6729. https://doi.org/
- Wu, H., Jagota, A., Hui, C.-Y., 2022a. Lubricated sliding of a rigid cylinder on a viscoelastic half space. Tribol. Lett. 70, 1. https://doi.org/10.1007/s11249-021-01537-4.
- Wu, H., Khripin, C., Jagota, A., Hui, C.-Y., 2022b. Enhancement of hydrodynamic friction by periodic variation of contact stiffness. Extreme Mech Lett 54, 101735. https://doi.org/10.1016/j.eml.2022.101735.
- Wu, H., Moyle, N., Jagota, A., Hui, C.-Y., 2020. Lubricated steady sliding of a rigid sphere on a soft elastic substrate: hydrodynamic friction in the Hertz limit. Eur. Phys. J. E Soft Matter. https://doi.org/10.1039/C9SM02447F, 10.1039.C9SM02447F.
- Wu, H., Moyle, N., Jagota, A., Khripin, C.Y., Bremond, F., Hui, C.-Y., 2019. Crack propagation pattern and trapping mechanism of rolling a rigid cylinder on a periodically structured surface. Extreme Mech. Lett. 29, 100475 https://doi.org/10.1016/j.eml.2019.100475.
- Zhang, Z., Bertin, V., Arshad, M., Raphaël, E., Salez, T., Maali, A., 2020. Direct measurement of the elastohydrodynamic lift force at the nanoscale. Phys. Rev. Lett. 124, 054502 https://doi.org/10.1103/PhysRevLett.124.054502.